Int J Adv Manuf Technol (2011) 55:95–106
DOI 10.1007/s00170-010-3023-6

ORIGINAL ARTICLE

Study on forming defects in the rolling process of large aluminum alloy ring via adaptive controlled simulation

Jie Zhou · Feng-lin Wang · Meng-han Wang · Wu-jiao Xu

Received: 1 June 2010 / Accepted: 3 November 2010 / Published online: 25 November 2010

Abstract According to the distribution characteristics of equivalent plastic strain (PEEQ) in radial–axial ring rolling, the plastic deformation zones in cross section were established. A 3D rigid-viscoplastic finite element model (FEM) which was controlled adaptively was applied to investigate defects that occurred during ring rolling under ABAQUS software. PEEQ, stress, and temperature distributions in different deformation zones have been analyzed in this study. Strain peaks were found in the cross-section corners. Moreover, it was investigated that non-uniform strain, stress, and temperature distributions in the ring tend to cause non-uniform microstructure and properties. Therefore, forming defects and microstructure damage would appear in cross-section corners due to the high-strain deformation. Based on the new developed FEM of the radial–axial ring-rolling process and comprehensive numerical simulations, the size effects of feed rate and lubrication conditions on strain and temperature distributions and their uniformity were investigated by 3D coupled thermomechanical FE simulation. The results have good agreement with experiment. The achievements of this study can provide basis for quality control and technical guidance.

Keywords Ring rolling · Plastic deformation zones · FEM · Defects · Deformation behaviors

J. Zhou · F.-l. Wang (✉) · M.-h. Wang · W.-j. Xu
School of Materials Science and Engineering,
Chongqing University,
ChongQing 400044, China
e-mail: wfltrees@163.com

1 Introduction

Ring rolling is used to manufacture a wide variety of mechanical components, ranging from small parts in bearings to large-scale parts used in power-generation plants, aircraft engines, large cylindrical vessels, and nuclear industries. The advantages for employing ring rolling include a short production time, uniform quality, smooth surface, close tolerance, and considerable savings in material cost.

The process of radial–axial ring rolling is highly nonlinear deformation behavior which contains material nonlinearity, contact nonlinearity, and geometry nonlinearity, and both microstructure and boundary conditions are altered by plastic deformation and recrystallization during hot ring-rolling process. Microstructure evolution in the hot ring-rolling process has a strong influence on the deformation behaviors because the flow stress is affected by dynamic recovery, dynamic recrystallization, and grain growth [1].

There have been a number of attempts to model the ring-rolling process using both two- and three-dimensional finite element (FE) techniques. Joun et al. [2] presented a new method for approximately predicting the deformation of material in ring-rolling process. The unknown variables, material velocity and tool velocity were determined. Utilizing this new approach based on a two-dimensional (2D) finite element method to perform shape design in ring rolling of bearing race. Kim et al. [3] firstly used the first 3D rigid-plastic finite element code "RING" to analyze non-steady state ring-rolling process. A spatially fixed mesh system including deforming region of the workpiece was constructed and good agreement between the simulation results and experiments was obtained in terms of

geometrical changes of rings in plain ring rolling and T-shaped profiled ring rolling. Wang min [4] used a coupled thermal–mechanical dynamic explicit FE model (FEM) to analyze the hot radial ring-rolling process. Two cases of hot plain ring rolling were simulated and the predicted material flow and temperature distribution of the ring are compared with experimental results. Davey et al. [5], concerned with a new approach founded on a split-operator arbitrary Lagrangian-Eulerian (ALE) formulation which combined with a flow formulation and a novel iterative solution scheme. Considerable run time benefits were achieved and the resulting model gave good predictions of both radial and axial flow, and ring growth. Alfozan et al. [6] used the upper bound element technique to determine the optimum intermediate shape for profile ring rolling using backward simulation. The simulation of the profile ring rolling was tested with different profiles of rolls and the presented method was validated using an experimental radial ring-rolling mill. The possibilities of foldovers, localized deformation, unwanted internal shearing, and improper roll fill could be avoided by the backward simulation technique. Xie et al. [7] used a rigid-viscoplastic dynamic explicit finite element code, H-RING, to analyze ring-rolling process, the cause and elimination of fishtail defect in rectangular section ring rolling and the strain distribution in L-section profiled ring rolling were investigated, three measures were suggested to eliminate the fishtail defect. Yea et al. [8] used a commercial FEM code, SHAPE-RR™ to simulated plain and T-shape rings by changing feed-rate and groove factor, the ring spread, pressure distribution, and roll force in plain and T-shape ring-rolling process were predicted. Koo et al. [9] analyzed an aluminum ring-rolling process using a rigid-thermoplastic finite element method. Forouzan et al. [10] investigated the performance of the "Thermal Spokes Method" in modeling the effect of the guide rolls on the ring-rolling process, and the reasons why thermal spokes were included in the FE model were presented. Much closer predictions for the lateral spread and low patterns were calculated and the tilting of the ring was predicted since the proposed method considered the effect of the guide rolls.

Moon et al. [11] applied a rigid-viscoplastic finite element method to investigate polygonal-shaped defects that occur during ring rolling. An improved analysis model with relatively fine finite elements was developed to minimize the volume change and reduce the computational time. The formation of a polygonal-shaped defect during hot ring rolling of a ball bearing outer race was simulated. Xu et al. [12] analyzed the evolution of the microstructure during hot ring rolling by means of proposed model employing a coupled thermomechanical three-dimensional rigid-plastic finite element method. The development of the microstructure was analyzed by mathematical models, careful control of some process parameters such as rolling speed, the temperature, and the cooling conditions could lead to fine grain size. Qian et al. [13] analyzed the plastic penetration using a three-dimensional finite element model, but both the rotations of main and the mandrel rollers were constrained in the FE model so that the unstable rolling process was replaced by a static upsetting process.

In this work, a new developed and adaptively controlled 3D coupled thermomechanical FE model was proposed. Then, based on the stable forming condition of the radial–axial ring-rolling process and comprehensive numerical simulations, the deformation behaviors and the root causes for forming defects of cross section were analyzed, size effects of processing parameters on equivalent plastic strain (PEEQ), temperature, and their uniformity were investigated. Experiments were conducted to validate the simulation results.

2 3D coupled thermomechanical FEM modeling of the ring-rolling process

2.1 FEM model of ring rolling

Ring rolling is a special rolling process in which a ring-shaped workpiece is drawn into the gap between the driven roll and the mandrel in order to cause material expanding in diameter and decreasing in thickness. The FEM model under ring-rolling process is shown in Fig. 1.

Due to ring vibration during processing, in order to keep the ring in central position and maintain circularity, the

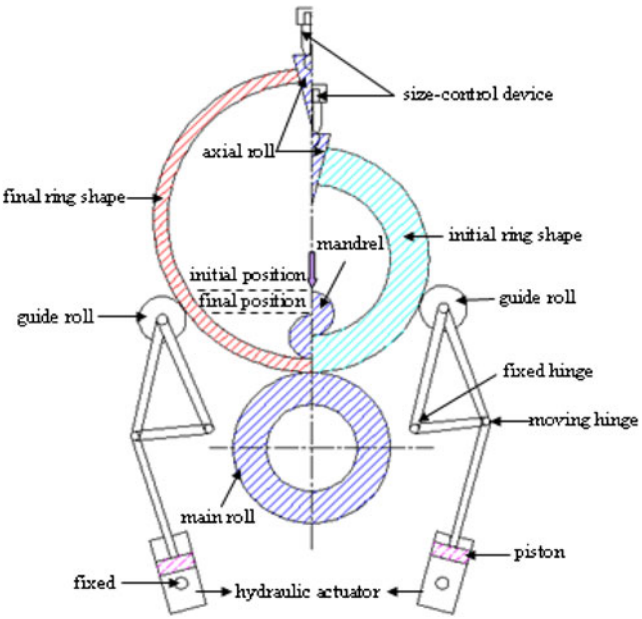

Fig.1 Schematic description of radial–axial ring rolling

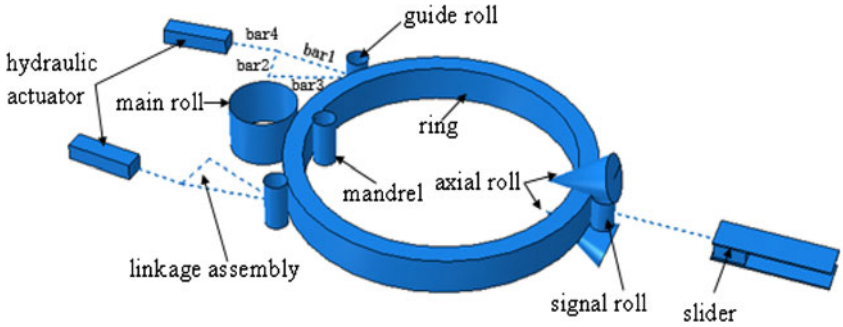

Fig. 2 FEM model of radial–axial ring rolling

guide rolls should be controlled by hydraulic adjustment mechanism adaptively. Figure 2 shows how a ring-rolling model is controlled adaptively.

Forouzan et al. (2003) [14] analyzed one kind of typical hydraulic adjustment mechanism of guide rolls. Li et al. (2005) [15] also researched guide roll control on the same mechanism. Literatures on the whole ring-rolling control method are relatively less. The developed and integrated FEM model is shown in Fig. 2. Different with former researches, the two guide rolls are controlled by each hydraulic ram respectively in this model. The weld connector elements are applied to weld three bars since the configurations of bar1, bar2, and bar3 are triangle shaped. The intersection point of bar2 and bar3 which is the circle center of guide roll pass is fixed. As bar4 can rotate relative to the triangle, the hinge connector element is used between bar4 and the triangle. Piston is located at the other end of bar4. With the growth of ring diameter, the hydraulic actuator would revolve around a fixed axis as shown in Fig. 1. Compared with single hydraulic actuator, the rational pressure on the two pistons can keep the guide rolls contacting with the ring and prevent the ring from tilting during the whole process since the pressure in each hydraulic ram could be set respectively according to the actual working condition. Thus, guide rolls control with more accuracy could be guaranteed.

The axial rolls are equipped with individual drives in order to minimize the surface speed mismatch between the ring and tapered axial rolls as the speed matching is significant for ring-rolling process. To guarantee the speed matching, a signal roll is added to this model, which is shown in Fig. 2. The signal roll is in contact with the ring during whole process, the expanding ring pushes the signal roll to move backward while the slider holds a resistant force. Whenever the signal roll moves backward, a feedback signal makes the axial rolls move backward simultaneously. Hence, the axial rolls and signal roll have the same movement speed as the equation constrain applied, and the rotate velocity of axial rolls is a function of rolling time. Therefore, the speed matching is excellent in this FEM model.

As kinematic nonlinearity method was applied during the analysis of ring-rolling process because of both contacting nonlinearity and material nonlinearity, the explicit dynamic FE procedure was used to simulate the ring-rolling process. Moreover, temperature-displacement coupled analysis was also applied in the simulation. A full Newton–Raphson iteration algorithm was chosen to solve the nonlinearity and a sparse direct solver was adopted to solve the simultaneous arithmetic equations. The workpiece was modeled using hexahedral elements with eight nodes. Initial Lagrangian mesh would be deformed or even be distorted excessively with the flow of materials which resulted that the solving would be aborted because of convergence problem. Hence, the adaptive mesh was applied in the ring-rolling process.

The ring material is aluminum alloy 7075 within 400–550°C forging temperature range. The thermal–mechanical property of aluminum alloy 7075 is listed in Table 1.The constitutive model used in this paper is Arrhenius model, which can be described by

$$\dot{\varepsilon} = f(\sigma)\ \exp(-Q/RT) \tag{1}$$

Where $f(\sigma)$ is stress function, which can be expressed as the following equation

$$f(\sigma) = A[\sinh(\alpha\sigma)]^n \tag{2}$$

Where A, α, σ, and n are constant. In order to reveal the synthetic effects of strain rate and temperature on flow

Table 1 Thermal–mechanical property of aluminum alloy 7075

Density	2,810 kg/m^3
Young's mould	72 GPa
Poisson's ratio	0.33
Specific heat	960 J/(kgK)
Thermal expansion	2.4E–5 1/K
Thermal conductivity	173 W/(mK)
Emissivity	0.7

Table 2 Values of coefficients in constitutive model for aluminum alloy 7075

α	7.905e-3
n	4.14
A	7.04e18
Q	2.32E5

stress, Zenr and Hollomon [16] presented the Z–H parameter which indicated temperature compensation strain rate. Z–H parameter satisfies the following equation:

$$Z = \dot{\varepsilon} \exp(Q/RT) \tag{3}$$

Where $\dot{\varepsilon}$ is the strain rate; Q is the deformation activation energy for aluminum alloy 7075; R is the gas constant; T is the absolute temperature. Substitute expression (2) and expression(3) into expression(1), it can be derived as Eq. (4):

$$\sigma = \frac{1}{\alpha} \ln\left\{ \left(\frac{Z}{A}\right)^{\frac{1}{n}} + \left[\left(\frac{Z}{A}\right)^{\frac{2}{n}} + 1 \right]^{\frac{1}{2}} \right\} \tag{4}$$

The values of the coefficients in above equations are shown in Table 2.

2.2 Key factors of thermomechanical coupling for FE modeling

2.2.1 Friction behavior

Six contact pairs are defined between the ring and the rolls, and friction between pressure plate and slider is existed. Relative sliding existing between the ring and rolls contributes to describe the friction with modified Coulomb friction model [17], namely

$$s = \begin{cases} \mu p & \text{if } s < s^* \\ s^* & \text{if } s \geq s^* \end{cases} \tag{5}$$

where s is the frictional stress, P is the contact pressure and s^* is the shear stress. The friction coefficient was analyzed based on the actual lubrication condition and experiment test data.

Table 3 Computational parameters for hot rolling of aluminum alloy 7075 rings

Forming parameters	Value
Driven roll diameter	φ1,200 mm
Mandrel roll diameter	φ450 mm
Guide roll diameter	φ320 mm
Cone angle of axial roll	40°
Initial ring outer diameter	φ4,300 mm
Initial ring inner diameter	φ3780 mm
Initial ring height	480 mm
Friction coefficient	0.35
Emissivity, ε	0.7
Convection coefficient, H_c	0.02N/s/mm/k
Contact heat conductivity, h_c	5 W/mm^2°C
Temperature of environment, T_f(°C)	25°C
Temperature of rolls, T_d (°C)	20°C
Initial temperature of ring, T_w (°C)	440°C

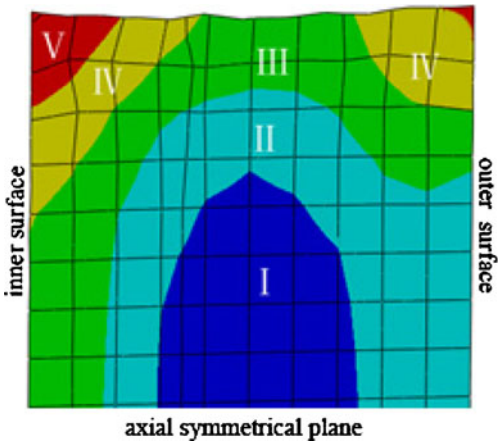

Fig. 3 Different deformation zones in cross section

2.2.2 Heat conduction

Besides friction factor, heat conduction at the interface of each contact pair between the ring and the rolls was also taken into consideration since the temperatures of ring and rolls were different. At each contact interface, contact heat conduction is assumed to be defined by

$$q = h(\theta_r - \theta_o)\ \dot{Q}_c = h_c A_c (T_w - T_d) \tag{6}$$

where $\dot{Q}_c$ is the heat flux crossing the interface from ring surface to roller surface, T_w and T_d are the temperatures of

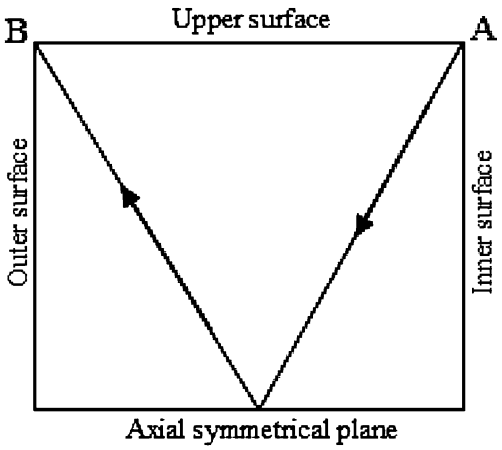

Fig. 4 Path from point A to point B in cross section

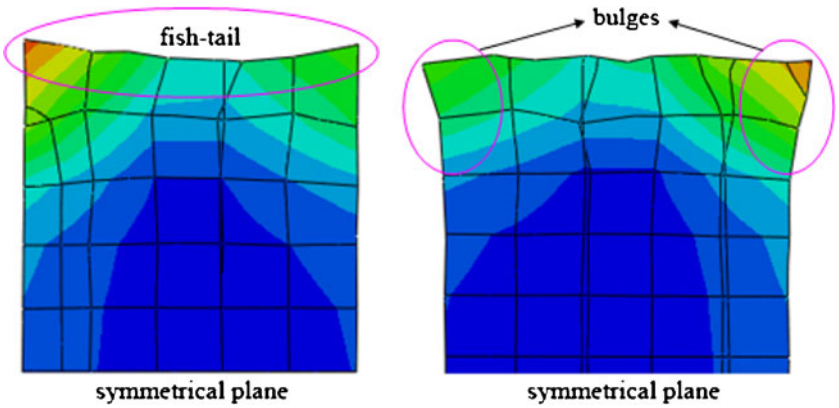

(a) fish-tail (b) bulges

Fig. 5 Forming defects in the cross section

the ring and rollers surfaces respectively, h_c is the contact heat conductivity, and A_c is the contact area.

2.2.3 Heat convection and heat radiation

The heat convection and radiation are considered on all the free surfaces of the ring. Heat radiation can take place as long as its temperature is above absolute zero. According to the Stefan–Boltzmann law, heat flux on each free surface due to radiation is governed by

$$\dot{Q}_r = \varepsilon\sigma_0 A_r\left(T_w^4 - T_f^4\right) \tag{7}$$

Where $\dot{Q}_r$ is the quality of heat by way of radiation; ε is the emmisivity; σ_0 is the Stefan-Boltzmann constant (σ_0= 5.6697e–008 $W/m^2{\cdot}K^4$); A_r is the radiation areas of ring and T_f is the ambient temperature.

For the heat convection, the heat flux is defined by

$$q_c = H_c(T_w - T_f) \tag{8}$$

Where q_c is the heat flux and H_c is the convection coefficient.

Table 3 summarizes the geometrical and computational parameters used in the FEM simulation.

3 Methodology of investigation

In order to analyze the deformation behaviors and defects of cross section more accurately, according to the simulation results, the different deformation zones in cross section were established. It was described as five typical deformation zones, as shown in Fig. 3. Different colors in the cross section represent different deformation zones. Besides, a path from point A to point B in the cross section of ring was defined for comparing the deformation behaviors with different rolling curves and process parameters, as shown in Fig. 4.

For a 3D coupled thermomechanical FEM model and considering the deformation behaviors in cross section of ring, it is necessary to obtain the variation laws of distributions of strain–stress and temperature. For simplicity, half of the ring cross section was taken into consideration since the deformations of ring rolling are mainly symmetric to the middle axial cross section, as shown in Figs. 3 and 4.

4 Results and discussion

4.1 Deformation behaviors in cross section

In terms of the forming principle of radial–axial ring rolling, the ring must go through two roll passes which are radial roll pass and axial roll pass respectively per revolution, which is different with purely radial or axial rolling. The deformation inhomogeneousness caused by non-uniform spreading is called “fishtail” according to its shape. The “fishtail” would occur after the radial deformation leading to bulges on the axial faces at the corners shown as in Fig. 5(a); These bulges are flattened but

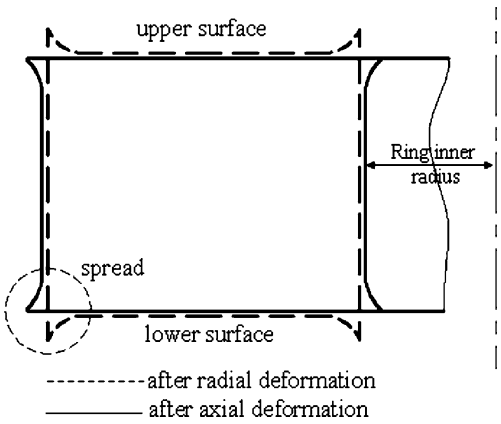

Fig. 6 Spread transformation of ring cross section

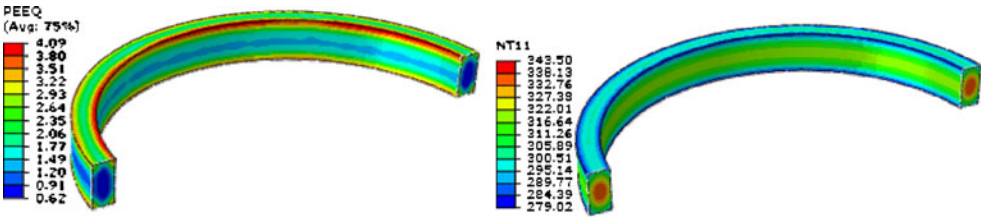

Fig. 7 PEEQ and temperature distribution in ring

reappeared on the radial faces after the axial deformation, as shown in Fig. 5(b).

The spread formed in radial pass is rolled off in the axial pass, and vice versa, as shown in Fig. 6. Thus high-strain deformations are induced around the two corners in each revolution of the ring. This alternating deformation of the bulges lead to excessive strain and forming energy concentration in the ring corners of the ring cross section. As a result, the strain and temperature are extremely non-uniform, as illustrated in Fig. 7, which may cause forming defects or microstructure damage.

4.2 Analysis of strain and stress distribution

The total equivalent plastic strain at the different five zones is shown in Fig. 8 as a function of rolling time.

As can be seen from Fig. 8, the strain distribution across the ring cross section is non-uniform since the external regions have higher levels of strain than that of inner region. Similarly, it can be seen that the strain concentration at the inner corner tends to be higher than that at the outer corner of the ring. This can be related to the small diameter and feed rate of the mandrel.

Figure 8 shows the PEEQ distribution in different zones of cross section. It can also be seen that the minimum strain occurred in middle areas of cross section. Moreover, the maximum strain is almost 3.5~8 times as large as the minimum strain. These appreciable differences lead to non-uniform microstructure between different deformation zones.

The Mises stress distributions observed within the roll gaps were plotted in Fig. 9. It can be concluded that the stress distributions had a similar variation with strain distributions, the stress values increase gradually from the internal to the external surface of the ring.

In the axial roll gap, the stress distribution concentrated near the upper and lower surfaces, which can be attributed to axial rolls. Furthermore, the maximum stress near upper surface is larger than that near the lower surface because the upper axial roll was given a downward velocity to realize axial deformation.

In addition, the variation rule of stress in the radial roll gap is the same as that in the axial roll gap. Because of the feed rate of mandrel and the driven force of main roll, plastic zones occur firstly on contact surfaces between rolls and ring, and then expand along opposite directions towards the middle radial layer of the ring until the two zones meet at an unpredictable location.

4.3 Analysis of new rolling curve

Based on the previous analysis of strain, temperature, and stress distribution in cross section, it is concluded that high-strain deformations are induced around the two corners in each revolution of the ring, which tends to cause severely non-uniform PEEQ, temperature and stress distribution, and it is main reason for forming defects. In order to avoid the alternating movement of the strain bulges during each revolution of ring, the new rolling curve was proposed, as shown in Fig. 10. The whole rolling process is divided into several continuous phases and deformations in radial and axial directions do not coincidentally exist within one phase. *H*0 and *B*0 are the initial thickness and height of billet. *H*f and *B*f are the final wall thickness and ring height respectively.

It is supposed that the rolling process begins with a phase (phase 1–2) of reducing the ring height. Since

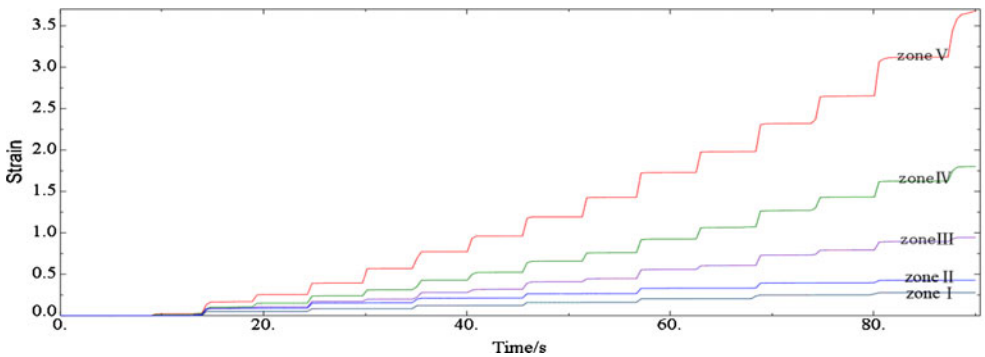

Fig. 8 Equivalent plastic strain at the different five zones

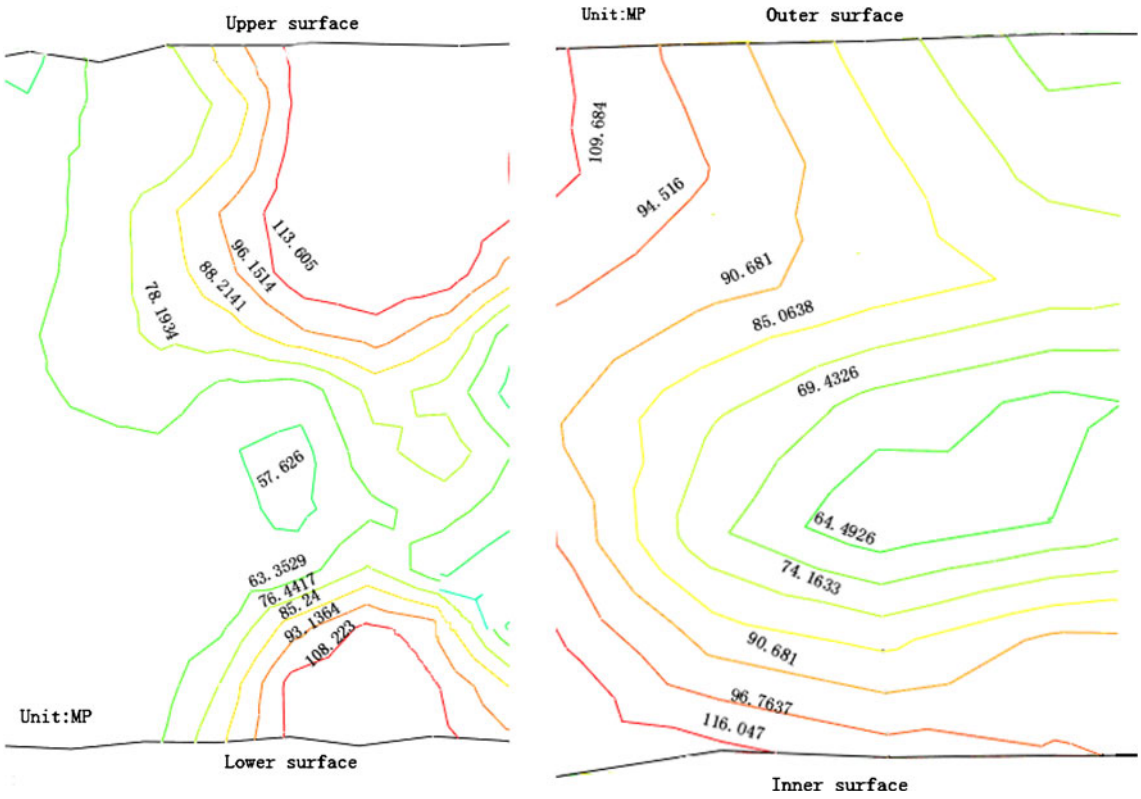

(a) axial roll pass (b) radial roll pass

Fig. 9 Stress contour line plot of the ring blank for a ring-rolling time of 60 s

deformation does not occur in the radial rolls during this phase, the existing spread triggers the wall thickness increasing. Then a phase (phase 2–3) of reducing wall thickness supervened after that and the axial rolls are guiding the ring with a certain minimum force. The radial and axial rolls are changed to active at the same time as soon as the dimensions of ring reach H or B (phase 9–10).

It can be seen from Fig. 11 that the PEEQ and temperature distributions with new rolling curve are more uniform than that with original rolling curve. This reveals that the new rolling curve can make more uniform microstructure and properties through decreasing the frequency of the bulge deformation.

4.4 Study of the mechanical and thermal behaviors of ring with different process parameters

The mechanical and thermal behaviors of ring during the radial–axial ring-rolling process lead to excessively non-uniform distribution of several variables, which would not only result in severely non-uniform microstructure and properties, additional tensile stress, etc., but also lead to forming defects occurrence like crack under some circumstances. Therefore, in order to study the effects of processing parameters on forming quality, the standard deviation was proposed to describe non-uniformity of strain and temperature distributions.

4.4.1 Evaluation indexes for the forming quality

The stand deviation of PEEQ and temperature are respectively denoted by $\mathrm{PEEQ_{sd}}$ and T_{sd}, defined as:

$$\mathrm{SD} = \sqrt{\sum_{i=1}^{n} (X_i - X_a)^2/(n-1)} \tag{9}$$

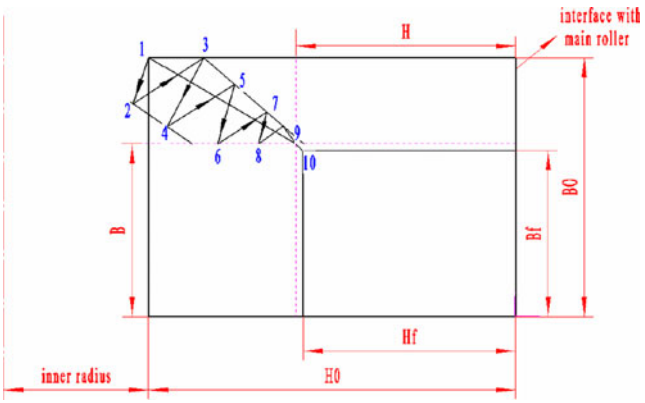

Fig. 10 The schematic diagram of new rolling curve

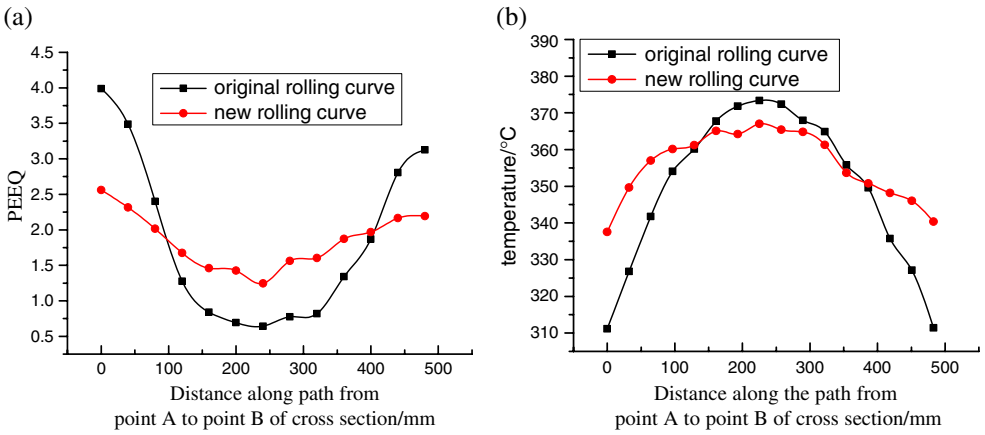

Fig. 11 Comparation of variables along the path with different rolling curve : **a** PEEQ distribution, **b** temperature distribution

Where X_i is the value of variable X at element i, X_a is the average of variable X, $X_a = \sum_{i=1}^{n} X_i/n$ and n is magnitude of variable.

4.4.2 The effect of $\Delta h/\Delta b$

Flow defects can be avoided by controlling the feed rates of the radial and axial rolls. The effect of $\Delta h/\Delta b$ (the ratio of radial to axial feed per revolution) on mechanical and thermal behaviors of was discussed in this paper and $\Delta h/\Delta b$ ranged between 0.14 and 0.82.

Figure 12a shows variations of $PEEQ_{sd}$ and T_{sd} with $\Delta h/\Delta b$, $PEEQ_{sd}$ and T_{sd} decrease with the increasing of $\Delta h/\Delta b$, and then an increase occurs, and the minimum occurs when the value of $\Delta h/\Delta b$ is equal to 0.54. PEEQ distributions along the path of cross section under various $\Delta h/\Delta b$ are shown in Fig. 12b. It is found that along the path of cross section, the minimum PEEQ exists in the middle layer while that in the inside and outside layers increases with decreasing $\Delta h/\Delta b$, thus resulting in an increasing $PEEQ_{sd}$, thereby leading to more non-uniform deformation. Temperature distributions along the path of

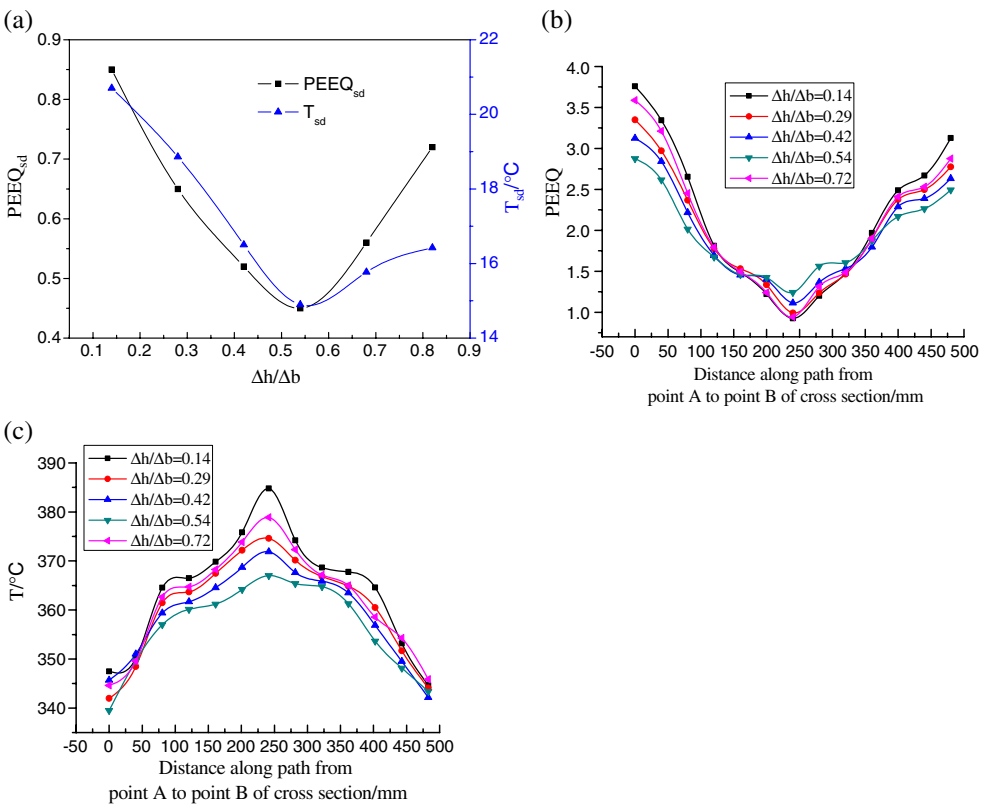

Fig. 12 Variations of mechanical and thermal behaviors with $\Delta h/\Delta b$: **a** variations of $PEEQ_{sd}$ and T_{sd} with $\Delta h/\Delta b$, **b** PEEQ distributions under various $\Delta h/\Delta b$, **c** temperature distributions under various $\Delta h/\Delta b$

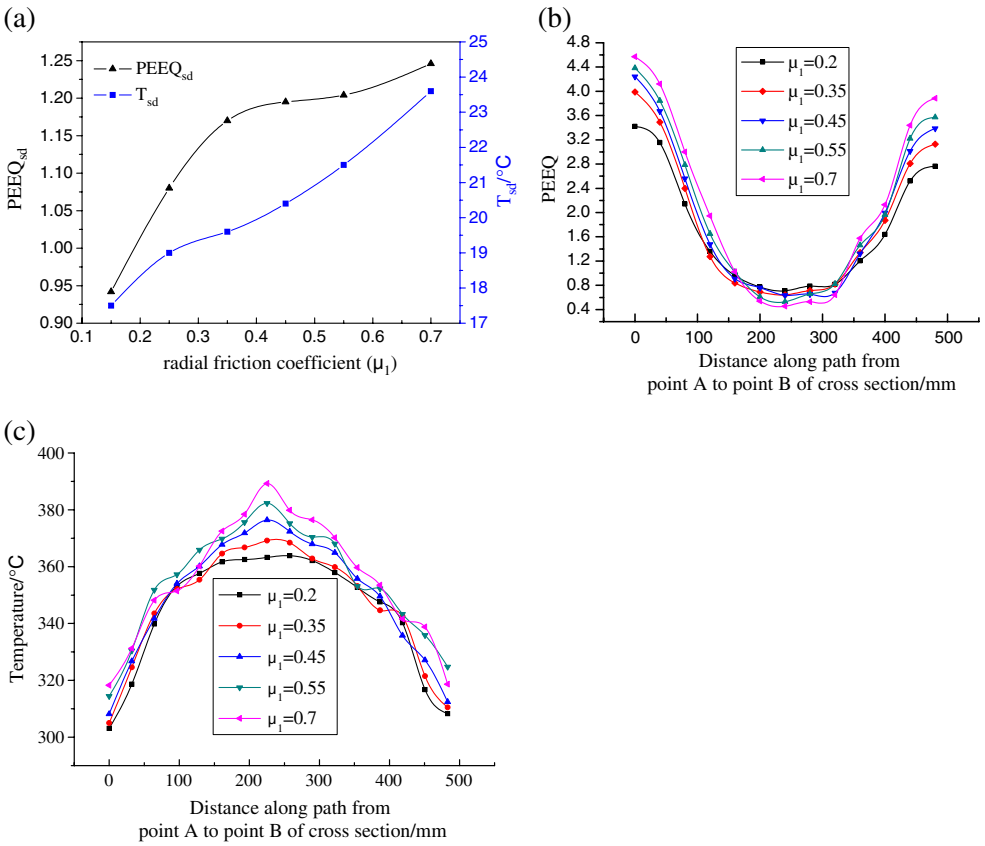

Fig. 13 Variations of mechanical and thermal behaviors with μ_1: **a** variations of $PEEQ_{sd}$ and T_{sd} with μ_1, **b** PEEQ distributions under various μ_1, **c** temperature distributions under various μ_1

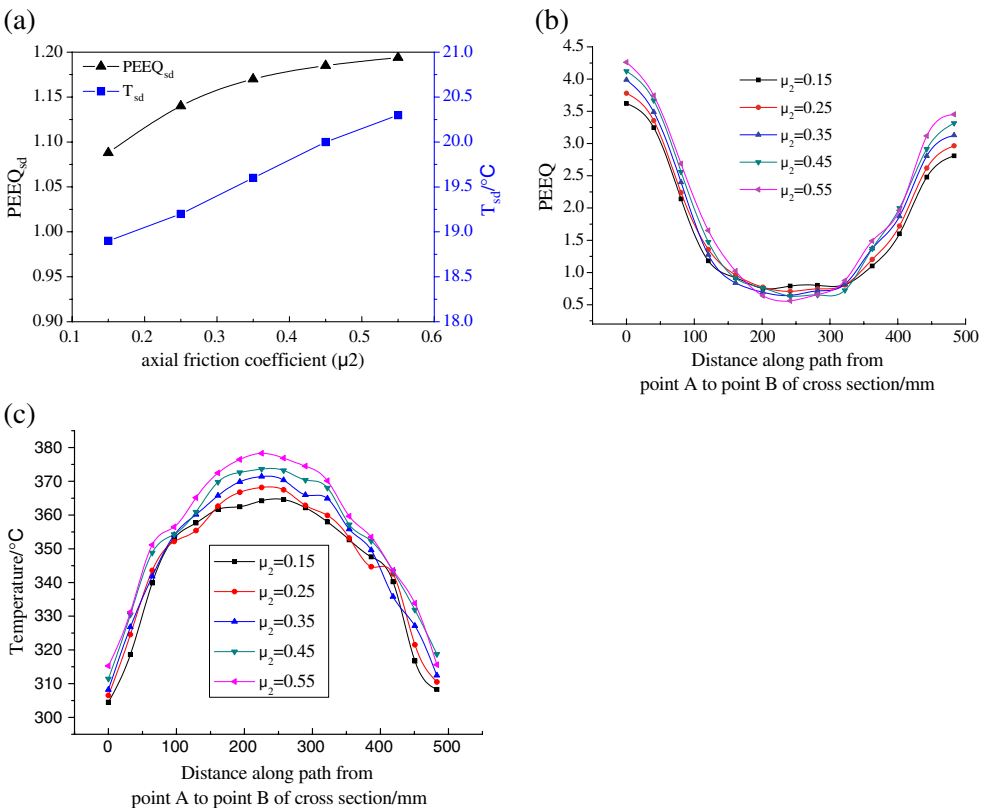

Fig. 14 Variations of mechanical and thermal behaviors with μ_2: **a** variations of $PEEQ_{sd}$ and T_{sd} with μ_1, **b** PEEQ distributions under various μ_2, **c** temperature distributions under various μ_2.

cross section under various $\Delta h/\Delta b$ are shown in Fig. 12c. It is found that temperature distributions have a similar variation to PEEQ distributions, thus causing T_{sd} to have a similar variation to $PEEQ_{sd}$.

4.4.3 The effect of radial friction coefficient μ_1

As we know, the lubrication condition plays an important role in ring-rolling process. Increasing the friction on the contact surfaces between rolls and ring is useful not only for improving the stability of ring rolling but also for improving the geometry and dimension precision of deformed ring. The effects of lubrication on deformation behaviors were studied in this article.

Figure 13a shows variation of $PEEQ_{sd}$ and T_{sd} with μ_1. $PEEQ_{sd}$ and T_{sd} increase with increasing μ_1. PEEQ distributions in ring under various μ_1 are shown in Fig. 13b. It was observed that the PEEQ in the middle layer decreases while that in the inside and outside layers increases with increasing μ_1, thus resulting in an increasing $PEEQ_{sd}$. Temperature distributions in ring under various μ_1 are shown in Fig. 13c. It was found that the temperature along the path of the cross section raised with increasing μ_1. Moreover, it could also be seen that the temperature rise in the middle layer is smaller than that in inside and outside layers, thus leading to increasing T_{sd}.

4.4.4 The effect of radial friction coefficient μ_2

Figure 14 shows variations of mechanical and thermal behaviors with μ_2. It was found that it had a similar variation to radial friction coefficient μ_1. Both the μ_1 and μ_2 had effects on mechanical and thermal behaviors of ring during ring-rolling process, It also could be seen μ_2 have an less influence on PEEQ and temperature distributions than μ_1 with the comparison between Fig. 13 and Fig. 14.

5 Experiment analysis

The experimental work has been carried out to validate the computed results of the forming defects simulation using adaptive control simulation. This was done on the 5 M radial–axial numerical control ring-rolling mill (maximum radial load 2,500 kN, maximum axial load 2,000 kN, maximum ring outer diameter 5 m) that has been fabricated in the South West Aluminum (Group) Ltd. (SWA) for experiment and production. The main components of radial–axial ring-rolling machine are shown in Fig. 15. The infrared thermometer DHS-200XEL was used to measure surface temperatures of rings without any contact.

The device for upsetting of initial billet(860 mm in diameter, 2,600 mm in height) is hydraulic press (maximum load is 6,000 t and the velocity of pressing is 85 mm/s), graphite(10%), cylinder oil(20%), and spindle oil(70%) were mixed to constitute the lubricant for piercing. The final rolled ring (5,050 mm in outer diameter, 210 mm in wall thickness and 440 mm in height) is sent for heat treatments. The main rolling parameters are as follows (Table 4):

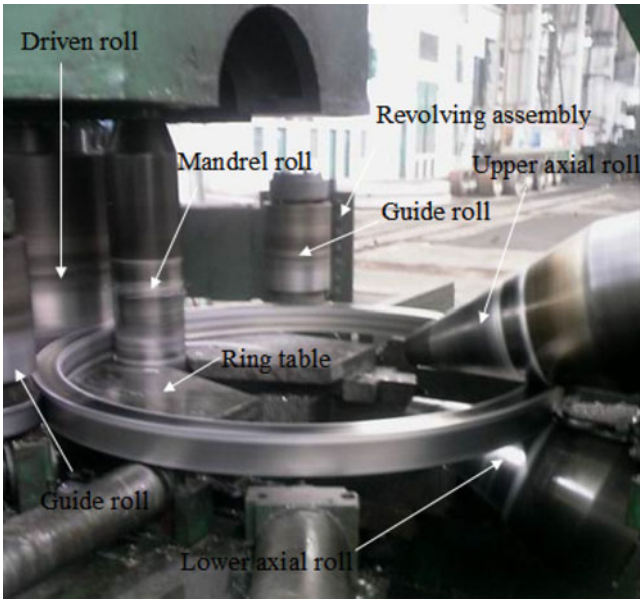

Fig. 15 Ring-rolling machine at south west aluminum (Group) Ltd (SWA)

Table 4 Experimental parameters for hot rolling of aluminum alloy 7075 rings

Forming parameters	Value
Relative reduction	0.24
Line velocity of main roller (mm/s)	1,300
Feed rate of idle roller (mm/s)	1.1
Initial temperature of ring (°C)	440
Temperature of rollers (°C)	20
Temperature of environment (°C)	30
Diameter of main roller (mm)	900
Diameter of idle roller (mm)	320
Diameter of guide rollers (mm)	320
Taper angle of axial rollers (mm)	40
Initial outer diameter of ring (mm)	4,130
initial thickness of ring (mm)	260
Initial height of ring (mm)	460
Radial rolling force (kN)	2,450
Axial rolling force (kN)	1,900
Maintaining force of guide rollers (kN)	35

Relative reduction=$(h_i-h_f)/h_f$, where h_i and h_f are the radial thicknesses of the initial and final rings, respectively.

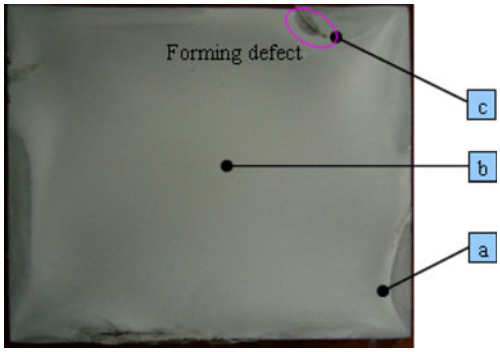

Fig. 16 The cross section of produced ring

The actual cross section of ring rolled shape is shown in Fig. 16. The forming defect was found in the corners of ring cross section, it has good agreement with the simulation results.

The high multiplying microstructure in different zones is shown in Fig. 17. It can be observed that the crystal grains in alternating deformation zone are as fine and homogeneous as the large volume fraction of dynamic recrystallization due to the large deformation.

While the volume fraction of dynamic recrystallization is very small owing to the low deformation, grain coarsening will occur because of the slow cooling speed in central zones, as shown in Fig. 17 b.

The different deformation degree in the cross section of ring lead to the unhomogeneous of crystal grain size, and the extravagant deformation would result in forming defect. As shown in Fig. 17c, the worse the strain distributes, the more non-uniform the microstructure becomes, which may lead to unsatisfied structure strength.

6 Conclusions

1. A full 3D coupled thermomechanical FEM model of ring rolling was built, which can guarantee more accuracy control due to the two guide rolls controlled by individual hydraulic actuator, respectively. The whole model was controlled adaptively.
2. The actual plastic deformation zones were established for analyzing deformation behaviors. The alternative deformation zones were found in the corners of ring cross section through simulation results.
3. A new rolling curve was proposed to decrease the alternating movement of the strain bulges during each revolution of ring, the simulation results showed that new rolling curve was beneficial to make more uniform PEEQ and temperature distributions. The effects of feed and lubrication condition on mechanical and thermal behaviors were studied.
4. The forming defects and low mechanical property would be triggered by the non-uniform equivalent plastic strain and temperature distributions due to the alternative deformation in the corners of cross section.

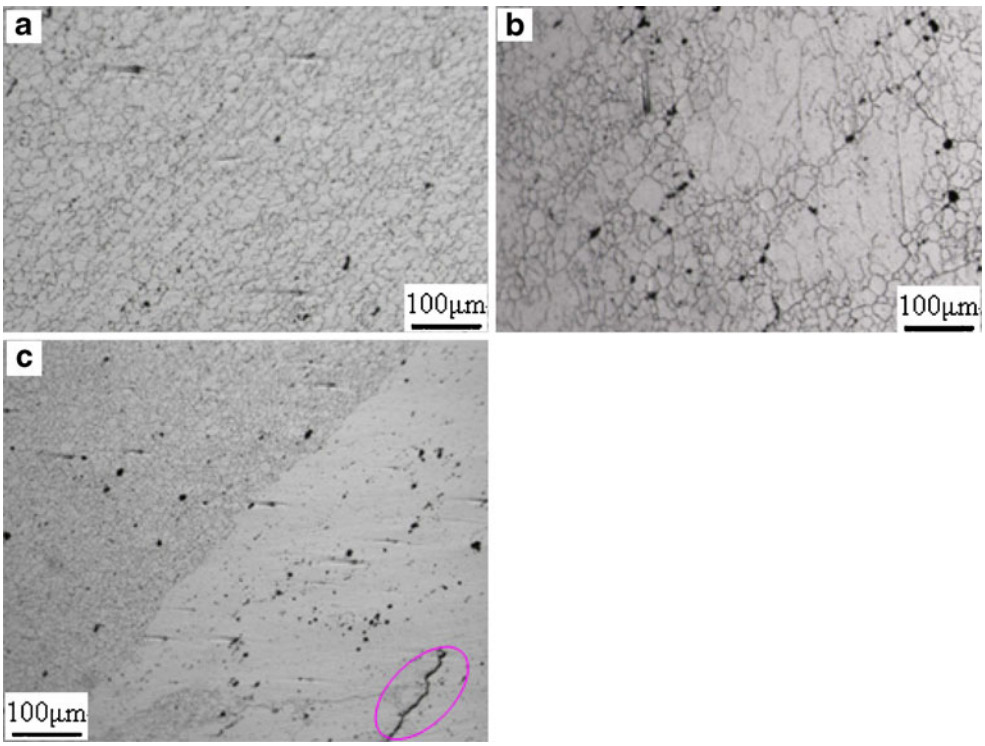

Fig. 17 High multiplying microstructure in different zones

Acknowledgements The authors would like to thank the support of Ministry of Science and Technology Sino-German Cooperation Project (2010DFA51860), Natural Science Foundation of Chongqing Key Project (No. 2009BA4065), and the Fundamental Research Funds for the Central Universities of China (CDJZR1013 0019).

References

1. Ma Q, Lin ZQ, Yu ZQ (2009) Prediction of deformation behavior and microstructure evolution in heavy forging by FEM. Int J Adv Manuf Technol 40:253–260
2. Joun MS, Chung JH, Shivpuri R (1998) An axisymmetric forging approach to preform design in ring rolling using a rigid–viscoplastic finite element method. Int J Mach Tools Manuf 38:1183–1191
3. Kim NS, Machida S, Kobayashi S (1990) Ring rolling process simulation by the three dimensional finite element method. Int J Mach Tools Manuf 30:569–577
4. Wang M, Yang H, Sun ZC, Guo LG, Ou XZ (2006) Dynamic explicit FE modeling of hot ring rolling process[J]. Trans Nonferrous Met Soc China 6(6):1274–1280
5. Davey K, Ward MJ (2003) An ALE approach for finite element ring-rolling simulation of profiled rings. J Mater Process Technol 139:559–566
6. Alfozan A, Gunasekera JS (2002) Design of profile ring rolling by backward simulation using upper bound element technique (UBET). J Manuf Process 4:97–108
7. Xie C, Dong X, Li S, Huang S (2000) Rigid–viscoplastic dynamic explicit FEA of the ring rolling process. Int J Mach Tools Manuf 40:81–93
8. Yea YS, Ko YS, Kim NS, Lee JC (2003) Prediction of spread, pressure distribution and roll force in ring rolling process using rigid-plastic finite element method. J Mater Process Technol 140:478–486
9. Koo SW, Lee JC, Yoon SJ, Kim NS (2003) Analysis of aluminum ring rolling process using thermo-rigid-plastic finite element method. Transactions of the Korean Society of Mechanical Engineers 27:815–822
10. Forouzan MR, Salimi M, Gadala MS (2003) Three-dimensional FE analysis of ring rolling by employing thermal spokes method. Int J Mech Sci 45:1975–1998
11. Moon HK, Lee MC, Joun MS (2008) Predicting polygonal-shaped defects during hot ring rolling using a rigid-viscoplastic finite element method. Int J Mech Sci 50:306–314
12. Xu SG, Cao QX (1994) Numerical simulation of the microstructure in the ring rolling of hot steel. J Mater Process Technol 43:221–235
13. Qian DS, Hua L, Zuo ZJ (2007) Investigation of distribution of plastic zone in the process of plastic penetration. J Mater Process Tech 187:734–737
14. Forouzan MR, Salimi M, Gadala MS, Aljawi AA (2003) Guide roll simulation in FE analysis of ring rolling. J Mater Process Technol 142:213–223
15. Li LY, Yang H, Guo LG, Sun ZC (2008) A control method of guide rolls in 3D-FE simulation of ring rolling. J Mater Process Technol 205:99–110
16. Zenter C, Hollomon H (1994) Effects of strain rate upon plastic flow of steel [J]. J Appl Phys 15:22–32
17. Gearing BP, Moon HS, Anand L (2001) A plasticity model for interface friction:application to sheet metal forming. Int J Plast 17:237–271